Ecological and Morphological Principles, K. V. Skufin, E. P. Narchuk, O. P. Negrobov, Eds. (Oxonian Press, New Delhi, India, 1985), pp. 56–59.
30. D. Grimaldi, *Bull. Am. Mus. Nat. Hist.* **195**, 164 (1990).
31. M. G. Mostovski, *Paleontl. J.* **1**, 72 (1997).
32. J. Zhang, S. Zhang, L. Y. Li, *Acta Palaeontol. Sin.* **32**, 662 (1993).
33. S. Y. Duan, *Sci. China Ser. D* **41**, 14 (1998).
34. D. A. Russell, *Can. J. Earth Sci.* **30**, 2002 (1993).
35. I am particularly grateful to an anonymous reviewer for critical review of the manuscript. The work was supported by the National Natural Science Foundation of China; the Fund for Young Geologists of the Ministry of Geology and Mineral Resources (MGMR); the Young Scientists Laboratory of Plant Origin and Environmental Changes, Chinese Academy of Sciences; the Special Fund (from the Financial Ministry) of Biological Sciences and Technology, Chinese Academy of Sciences; and the Laboratory of Geomechanics, MGMR.

28 October 1997; accepted 13 February 1998

Capture of Interplanetary and Interstellar Dust by the Jovian Magnetosphere

Joshua E. Colwell,* Mihály Horányi, Eberhard Grün

Interplanetary and interstellar dust grains entering Jupiter's magnetosphere form a detectable diffuse faint ring of exogenic material. This ring is composed of particles in the size range of 0.5 to 1.5 micrometers on retrograde and prograde orbits in a 4:1 ratio, with semimajor axes $3 < a < 20$ jovian radii, eccentricities $0.1 < e < 0.3$, and inclinations $i \lesssim 20$ degrees or $i \gtrsim 160$ degrees. The size range and the orbital characteristics are consistent with in situ detections of micrometer-sized grains by the Galileo dust detector, and the measured rates match the number densities predicted from numerical trajectory integrations.

The dust detector on the Galileo spacecraft (DDS) measures impacts of dust particles and gives estimates of the masses and the velocities of the grains (*1*). Grains were detected by the DDS inside about 20 Jovian radii (R_J; 1 R_J = 7.1492 × 10^4 km) on prograde and retrograde orbits around Jupiter (*2*). These grains are at least several tenths of a micrometer in radius.

During Galileo's second orbit, eight "large" dust grains were detected inside 20 R_J, and, based on the rotation angle of the detector and the impactor speeds, most of these particles follow retrograde orbits (Fig. 1). The impact rate of these particles on the detector was $I \approx 3 \times 10^{-5}$ s^{-1}. Similar numbers were seen on subsequent orbits. The number density of uniformly distributed particles on circular Keplerian orbits necessary to explain this impact rate is $n_{DDS} \approx I/\sigma(f_p/v_p + f_r/v_r)$, where σ is the effective cross section of the DDS, f_p and f_r are the fraction of detected grains on prograde and retrograde orbits, respectively, and v_p and v_r are the relative velocities. We used the physical cross section $\sigma = 10^3$ cm^2 (*3*). Using circular Keplerian orbits for the dust at 15 R_J (roughly the middle of the region where the large grains were detected), $n_{DDS} \approx 10^{-14}$ cm^{-3}, which implies a mean optical depth of $\tau_{dust} \lesssim 10^{-11}$. Captured interstellar and interplanetary grains and the jovian moons are potential sources of these grains.

To determine these sources, we integrated the trajectories of dust grains in Jupiter's magnetosphere, using the same numerical approach as in our earlier studies (*4*). The grains move under the influence of Jupiter's and the sun's gravity, solar radiation pressure, and the Lorentz force. The grain's charge is time-dependent and is calculated from the current balance equation $dQ_{dust}/dt = \Sigma_i I_i$, where I_i is electron and ion thermal currents and secondary and photoelectron emission currents. The currents are all functions of the grain's velocity and position in the magnetospheric plasma and of the instantaneous charge on the grain which is assumed to have a density of 1.0 g cm^{-3}.

Our magnetospheric model uses Voyager plasma parameters (*5*–*6*) outside 5 R_J and an "engineering" plasma model (*7*) inside 5 R_J. The magnetic field is the O6+ current sheet model, assuming rigid corotation up to a distance of $R = 50$ R_J from Jupiter's center (*8*). Outside 50 R_J, we assumed solar wind conditions and reversed the azimuthal component of the magnetic field in 14-day intervals to imitate the sector structure of the interplanetary magnetic field (Fig. 2). There is no magnetotail or bow shock in this model. Grains were started with an initial potential of +5 V, the equilibrium value in the solar wind (*9*), at a distance of 100 R_J from Jupiter. We followed the particles until they either hit Jupiter, were more than 300 R_J from Jupiter, or 5 (Earth) years had passed. The fraction of captured grains and their orbital parameters enable us to estimate the number density of dust orbiting Jupiter from each of the possible sources.

Dust particles in the solar wind develop a positive charge and experience a retarding force entering Jupiter's magnetosphere because of the outward-pointing, corotating jovian electric field. On the outbound portion of their trajectory, dust grains regain some, but not all of their energy because of charging time delays. The grains' dynamical time scales are shorter than the charging time scales, so in general, they are not in charge equilibrium with the plasma in the jovian magnetosphere (*10*). Simultaneously, their angular momentum decreases. Similarly, grains within the jovian magnetosphere can also lose or gain energy and angular momentum leading to rapid changes of grain semimajor axis and eccentricity. The process is dependent on the size of the grains, which determines their charge-to-mass ratio and susceptibility to radiation pressure and the Lorentz force. Particles that experience this rapid loss of energy and angular momentum become captured in Jupiter's magnetosphere, where their lifetime is limited by sputtering, plasma drag, or collision with a moon or Jupiter (9).

Measurements of dust impacts by Galileo and Ulysses during interplanetary cruises showed that beyond about 3 astronomical units (1 AU = 1.49 × 10^{13} cm) the flux of submicrometer-sized dust particles is dominated by interstellar grains, with a flux of $F_{is} = 10^{-8}$ cm^{-2} s^{-1} in the same direction as the local interstellar wind (*11*). The mean mass of these particles is $10^{-12.5 \pm 1.5}$ g, and their approach speed to Jupiter varies from about 13 to 39 km s^{-1} as Jupiter orbits the sun.

We computed the trajectories of grains with sizes of 0.4 to 1.0 μm in 0.1-μm increments, with 10,000 particles at each size (*12*). The grains were started with impact parameters randomly distributed between 0 and 10 R_J, with a uniform surface density (*13*). Trajectories were integrated at three different approach velocities corresponding to upstream (Jupiter's orbital velocity antiparallel to the dust velocities), downstream, and cross-stream geometries with respect to the flow of interstellar gas through the solar system.

The most grains captured at any size were nine of the 0.6-μm grains in the downstream geometry. In the same geometry, three of the 0.5-μm grains were captured and one each at 0.7 and 0.8 μm. The capture efficiency as a function of particle size therefore peaks at 9 × 10^{-4} for 0.6-μm

J. E. Colwell and M. Horányi, Laboratory for Atmospheric and Space Physics, University of Colorado, Boulder, CO 80309–0392, USA.
E. Grün, Max Planck Institut für Kernphysik, 6900 Heidelberg, Germany.

*To whom correspondence should be addressed. E-mail: colwell@casper.colorado.edu

grains. The overall capture efficiency for a size distribution of interstellar grains is less than this peak capture efficiency and depends on the detailed size distribution of the incoming particles. Assuming that the interstellar dust size distribution peaks near 0.5 μm [$10^{-12.3}$ g; the measured value is $10^{-12.5 \pm 1.5}$ g (*11*)], we estimate a lower limit for the total capture efficiency $f_{c,is} \approx 10^{-4}$ in the downstream direction, based on our integrations. The capture efficiency is highest in this geometry, because the speed of the interstellar dust relative to Jupiter is minimized, and the particles must lose less energy to be captured than when Jupiter's orbit velocity carries it into the interstellar wind. Accounting for the fraction of Jupiter's orbit that is approximately in this geometry relative to the interstellar dust, we take $f_{c,is} = 10^{-5}$ as an order-of-magnitude lower limit estimate.

The average capture rate of interstellar grains by Jupiter's magnetosphere is $\dot{N}_{is} = AF_{is}f_{c,is} = 1.6 \times 10^9$ s^{-1}, where $A = \pi(10\ R_J)^2$ is the cross-sectional area of the region our test grains were sent in order to empirically determine $f_{c,is}$. We found that most captured grains have stable orbits with semimajor axes (a) between 3 and 15 R_J, eccentricities (e) between 0.1 and 0.3, and inclinations (i) of <20° or >160° (Fig. 3). This gives a toroidal volume of space occupied by the captured grains between 3 and 20 R_J with a volume $V \approx 4 \times 10^{33}$ cm^3. The average number density of grains in this volume is $n_{is} = \dot{N}_{is}T/V$, where T is the lifetime of the grains.

Our orbital integrations show that the orbits are dynamically stable for longer than 100 years, so the loss time scale is set by plasma drag, collisions, sputtering, or evaporation. The time scale for loss of micrometer-sized grains from the main Jovian ring because of these processes is $T \gtrsim 100$ years (*14*). Using Öpik's formalism (*15*), we find $T_{coll} = 34$ years for a particle on a retrograde orbit with $i = 160°$, $e = 0.3$, and $a = 15\ R_J$ for collisions with Ganymede ($a_{Ganymede} = 15\ R_J$), and $T_{coll} = 85$ years for the same particle on a prograde orbit. Because the orbital elements of the grains vary with time and dynamically longer lived orbits exist between the Galilean satellites, we adopt $T = 100$ years. This gives $n_{is} = 1.3 \times 10^{-15}$ cm^{-3}.

We modeled the interplanetary population of dust at Jupiter with a "planetary" population consisting of particles on low-e, low-i orbits and an "Oort Cloud" population consisting of particles on isotropically distributed near-parabolic orbits (*4, 16*). We used an interplanetary flux model (*17*) to estimate the contribution of interplanetary dust to the total flux of 0.5- to 1.5-μm grains at Jupiter of $F_{planetary} = 3 \times 10^{-11}$ cm^{-2} s^{-1} and $F_{Oort} = 3.2 \times 10^{-10}$ cm^{-2} s^{-1}.

Grains were captured from the planetary population at all sizes from 0.4 to 2.0 μm with a typical efficiency of $f_{c,p} = 10^{-3}$. The peak capture rate was for 0.8-μm grains, where $f_{c,p} = 3 \times 10^{-3}$; most captured grains were between 0.6 and 1.4 μm. Computing the number density interior to 20 R_J for these grains in the same way as for the interstellar grains yielded $n_{planetary} = 4 \times 10^{-14}$ cm^{-3}. Because of the much higher approach speeds of cometary dust, we captured only one dust particle from a cometary orbit, starting with 10,000 grains at each particle size (*18*). Based on this single grain, $f_{c,0} \lesssim 10^{-5}$, and we can only estimate an upper limit on the abundance of cometary dust orbiting Jupiter: $n_{Oort} \lesssim 4 \times 10^{-15}$ cm^{-3}.

Micrometeoroid impact ejecta from the regular prograde satellites of Jupiter will similarly be on prograde orbits. The ejecta size distribution is a power law of the form $n(r)dr \propto r^{-q}dr$, where $q \approx 3.5$ is the size distribution index and r is the particle size (*19*). Thus, impact ejecta detected by the DDS should exhibit a broad size distribution contrary to the narrow distribution of sizes near 0.5 to 1.0 μm for the impacts studied here. Furthermore, we know of no mechanism—including angular momentum exchange with the magnetosphere—capable of reversing the orbital direction of dust on short-period prograde orbits. This leaves the four irregular retrograde satellites of Jupiter as the only endogenic source of retrograde dust in the Jupiter system (*20, 21*).

These satellites' a values lie between 296 and 332 R_J, their i values are between 147° and 163°, and their radii range from 15 to 35 km. Ejecta from these satellites are loosely bound to Jupiter and quickly perturbed by radiation pressure into high-e orbits. Most are lost from Jupiter's gravitational field of influence or strike Jupiter. However, because these grains start on orbits that have a low energy relative to Jupiter, they may be captured into small prograde or retrograde orbits through the same mechanism that captures interplanetary and interstellar grains.

The mass flux of micrometeoroids at Jupiter is dominated by 100-μm particles and is $F_m \approx 10^{-16}$ g cm^{-2} s^{-1} (*22*). The ejecta flux $F_{ej} = AYF_m$, where $Y = 10^3$ to 10^6

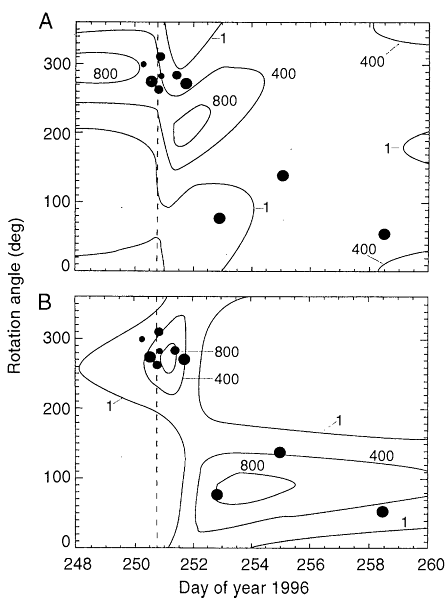

Fig. 1. (**A**) The large (micrometer-sized) particles detected by the Galileo DDS during the G2 encounter (flyby of Ganymede on Galileo's second orbit) showing the orientation of the DDS at each impact. Closest approach to Ganymede is indicated by the vertical dashed line. Distance from Jupiter of the Galileo spacecraft varied from a minimum of 10.7 R_J on day 251 to a maximum of 68 R_J on day 260. Dot sizes are proportional to particle mass, but the absolute calibration depends on impact velocity which is uncertain. The contours are DDS effective cross section for particles on circular prograde orbits in units of square centimeters. Most of the detected grains are far from the two peaks, suggesting they are not on prograde orbits. (**B**) The contours represent DDS effective cross section for particles on circular retrograde orbits. Most of the particles come from directions where the DDS has a high effective cross section for particles on retrograde orbits (*3*).

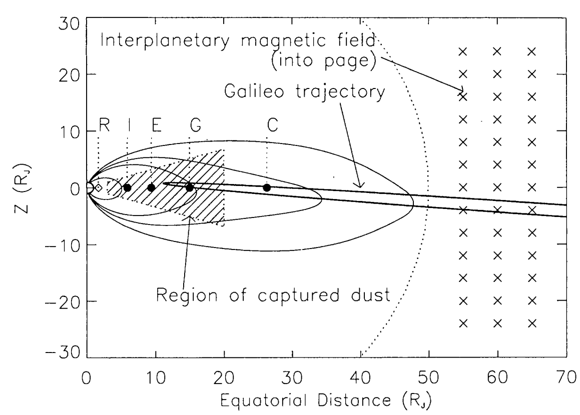

Fig. 2. A schematic cross section of the model jovian magnetosphere shows the main jovian ring (R), the Galilean satellites Io (I), Europa (E), Ganymede (G), Callisto (C), the trajectory of the Galileo spacecraft on the G2 orbit, the region of space occupied by captured interplanetary and interstellar dust, and the interplanetary magnetic field (crosses). The dotted line indicates the boundary of the model jovian magneto-sphere. All dust particle integrations started with dust at a distance of 100 R_J.

depends on surface properties of the moon (*23*, *24*), and A is the moon cross-sectional area. Using $q = 3.5$, the ejection rate of particles from each retrograde satellite in the 0.5- to 1.5-μm size range is $\dot{N}_{moon} \approx 1.2 \times 10^9 F_{ej}/(r_1^{3/2} - r_0^{3/2})$, where r_1 and r_0 are the largest and smallest particles ejected, respectively. Assuming r_1 is comparable to the size of the typical impactor ($r_1 = 100$ μm) and the smallest particles are smaller than 0.5 μm, the ejection rate for all four retrograde satellites is $\dot{N}_{moon} \approx 2 \times 10^{25}\, YF_m$ s^{-1}. If $Y = 10^6$ as appropriate for impacts into loose sand (*24*), then the mass loss rate from each satellite if reaccretion is negligible would result in complete erosion of the moon in less than the age of the solar system. Because the typical ejection velocity (*25*) exceeds the escape speed of the moons (11 m s^{-1}) and all ejecta produced by impacts are probably lost, a value of $Y = 10^3$ for a solid rocky or icy surface is appropriate. This gives $\dot{N}_{moon} \approx 2 \times 10^{12}$ s^{-1}.

We integrated the trajectories of 2500 particles at each size from 0.4 to 1.0 μm in 0.1-μm increments launched from Ananke, the innermost retrograde satellite, for 40 years or until the particles are more than 900 R_J from Jupiter (*26*). We found that the capture efficiency of particles into the orbits detected by the DDS is less than 3×10^{-4} resulting in a number density of dust in the 3- to 20-R_J region of $n_{moon} \lesssim 3 \times 10^{-16}$ cm^{-3}, much less than the number densities we obtained for the exogenic sources.

All the calculated and detected number densities of orbiting large grains can only be considered order-of-magnitude estimates because of our incomplete knowledge of the impacting flux, size distribution, and the orbital elements of the detected dust particles. However, our simulations indicate that interstellar and interplanetary grains can be captured on prograde and retrograde orbits, with an approximate preference of four to one for the latter case, and that these exogenic sources are the dominant source of micrometer-sized dust on retrograde orbits. The captured dust population is dominated by low-e interplanetary grains over interstellar grains by a factor of 30. We conclude that the capture of interplanetary and interstellar dust results in a tenuous ring around Jupiter composed of particles ~0.5 to 1.5 μm in radius. The average optical depth of this ring is $\tau \lesssim 10^{-11}$, and the number density is $n \sim 10^{-14}$ cm^{-3} in the region from 3 to 20 R_J. Particles in this ring of captured dust may have already been detected by the Galileo DDS. This ring is enhanced by stochastic events such as the capture of comet Shoemaker-Levy 9 into temporary orbit around Jupiter. This comet enhanced the flux of cometary dust at Jupiter, some of which may have been captured into retrograde orbits (*27*).

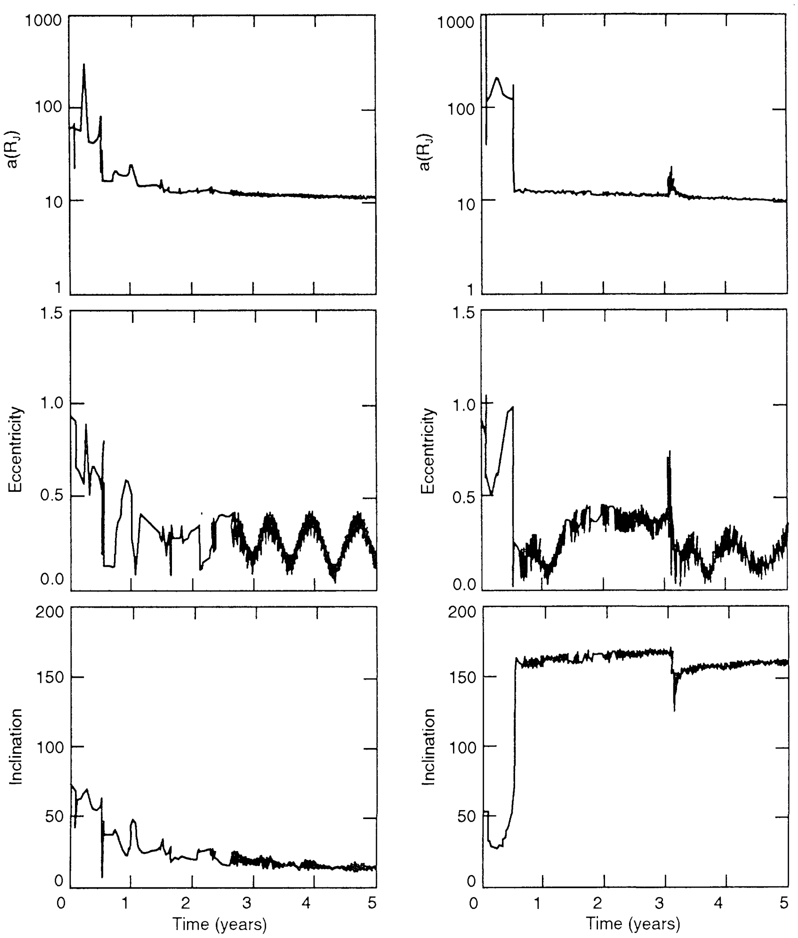

Fig. 3. The history of the orbital elements semimajor axis a (top), eccentricity e (middle), and inclination i (bottom) of two interstellar grains that became captured in Jupiter's magnetosphere on a prograde (left) and on a retrograde orbit (right). The orbits are stable, and the oscillation in the eccentricity is due to forced precession of the orbit by electromagnetic forces and Jupiter's oblateness and pumping of the eccentricity by radiation pressure (*28*). Some grains are captured into smaller orbits with $a \approx 3\ R_J$, whereas others are on larger orbits. Grains captured into orbits with $a > 25\ R_J$ were not considered in this discussion. The eccentricity of the grain on the right is gradually pumped up by radiation pressure, causing it to make a deep penetration into the jovian magnetosphere where it undergoes energy and angular momentum exchange leading to a small a and a retrograde orbit.

REFERENCES AND NOTES

1. E. Grün *et al.*, *Space Sci. Rev.* **60**, 317 (1992).
2. E. Grün *et al.*, *Geophys. Res. Lett.*, in press.
3. The physical cross section of the Galileo DDS is 1000 cm^2. However, because the detector is at the base of the cylindrical detector housing, the effective cross section is always smaller than the physical cross section and depends on the relative velocity of dust grains and the detector and the detector's orientation. For the purposes of calculating the detected number density of large grains, we used the physical cross section, because the effective cross section depends on the unknown orbit parameters of the detected grains. Figure 1 shows the effective cross section (in square centimeters) of the DDS for two different assumed orbits: circular prograde and circular retrograde. Because the effective cross section of the DDS is much higher for the retrograde orbit model than the prograde model, it is probable that the detected grains were on retrograde orbits. The probability that any one grain is on a retrograde rather than prograde orbit can be estimated from the ratio of effective cross sections for the two orbit models. Thus, the detection at day 253 and a rotation angle of 80° is approximately 800 times more likely to be of a grain on a retrograde rather than a prograde orbit.
4. J. E. Colwell and M. Horányi, *J. Geophys. Res.* **101**, 2169 (1996).
5. E. C. Sittler Jr. and D. F. Strobel, *ibid.* **92**, 5741 (1987).
6. F. Bagenal, in *Time Variable Phenomena in the Jovian System*, NASA Spec. Publ.-SP 494, M. J. S. Belton, R. A. West, J. Rahe, Eds. (NASA, Washington, DC, 1989).
7. N. Divine and H. B. Garrett, *J. Geophys. Res.* **88**, 6889 (1983).
8. This is a spherical harmonic expansion of the field to degree and order 6, using data from Pioneers 10 and 11 and Voyagers 1 and 2 [J. E. P. Connerney, *J. Geophys. Res.* **98**, 18659 (1993)].
9. M. Horányi, *Annu. Rev. Astron. Astrophys.* **34**, 383 (1996).
10. The time to reach approximate charge equilibrium for a 1-μm grain at the orbit of Ganymede is tens of minutes. Grains on eccentric orbits move through

the inhomogeneous plasma of the Jovian magnetosphere and, in general, are not in charge equilibrium with the local plasma environment. At any time, the charge on the grain is determined by currents due to the local plasma environment and the charge acquired in other environments encountered earlier. This charge memory makes the grain charging history irreversible and therefore nonconservative, so that energy and angular momentum may be gained from or lost to the magnetosphere.

11. M. Baguhl *et al.*, *Space Sci. Rev.* **72**, 471 (1995).
12. Here, grain size refers to the radius of spherical particles. We used smaller interstellar dust particles than interplanetary dust particles, because the higher velocity (energy) of the interstellar grains relative to Jupiter requires a stronger electromagnetic interaction with the magnetosphere for capture to occur. Numerical integrations of test particles confirmed that larger interstellar dust particles cannot lose enough energy to become captured, whereas smaller interstellar dust particles have enough kinetic energy to penetrate deep into the jovian magnetosphere, where energy and angular momentum exchange can lead to capture.
13. A 10-R_J target area was used for interstellar dust, because their higher velocities relative to Jupiter mean that only particles on near-miss trajectories can be captured. Numerical integrations of test particles with larger impact parameters showed that they are not captured. A smaller area was used to improve capture statistics.
14. J. A. Burns, M. R. Showalter, G. E. Morfill, in *Planetary Rings*, R. Greenberg and A. Brahic, Eds. (Univ. of Arizona Press, Tucson, AZ, 1984), pp. 200–272.
15. E. J. Öpik, *Proc. R. Ir. Acad.* **54**, 165 (1951).
16. J. E. Colwell, *Icarus* **106**, 536 (1993).
17. N. Divine, *J. Geophys. Res.* **98**, 17029 (1993).
18. The cometary orbits are for long-period Oort-cloud comets. Velocities of cometary dust relative to Jupiter in this model range from 8 to 34 km/s (planetary dust approach velocities are between 6 and 10 km/s). Heliocentric orbital elements are appropriate for dust released from an Oort-cloud comet: a = 20,000 to 40,000 AU, e = 1 to 1 – (5.2 AU/a), and cos i randomly distributed between –1 and 1 (*4*).
19. N. Asada, *J. Geophys. Res.* **90**, 12445 (1985).
20. H. A. Zook and S. Su, *Lunar Planet. Sci.* **XIII**, 893 (1982). The four retrograde satellites are Ananke ($a = 21.2 \times 10^{11}$ cm, $e = 0.169$, $i = 147°$, r = 15 km), Carme ($a = 22.6 \times 10^{11}$ cm, $e = 0.207$, $i = 163°$, r = 22 km), Pasiphae ($a = 23.5 \times 10^{11}$ cm, $e = 0.378$, $i = 148°$, r = 35 km), and Sinope ($a = 23.7 \times 10^{11}$ cm, $e = 0.275$, $i = 153°$, r = 20 km).
21. H. A. Zook, S. Su, D. D. Humes, *Lunar Planet. Sci.* **XVI**, 946 (1985).
22. E. Grün, H. A. Zook, H. Fechtig, R. H. Giese, *Icarus* **62**, 244 (1985).
23. D. E. Gault, *Moon* **6**, 32 (1973).
24. D. Stöffler, D. E. Gault, J. Wedekind, G. Polkowski, *J. Geophys. Res.* **80**, 4062 (1975).
25. K. R. Housen, R. M. Schmidt, K. A. Holsapple, *ibid.* **88**, 2485 (1983).
26. Particles launched from the retrograde jovian satellites are already bound to Jupiter, and their orbital evolution is much slower than that of exogenic grains that pass through the entire magnetosphere in one orbit. Computation time constraints limited the number of such particles at each size to 2500. Enough integrations were performed to arrive at an upper limit of capture efficiency of such grains into small retrograde orbits like those detected by the Galileo DDS.
27. M. Horányi, *Geophys. Res. Lett.* **21**, 1039 (1994).
28. ______ and J. A. Burns, *J. Geophys. Res.* **96**, 19283 (1991).

29. Partially supported by NASA. G. Linkert and H. Krüger assisted in Galileo data reduction and A. Heck assisted in figure preparation.

24 October 1997; accepted 18 February 1998

Time Scales and Heterogeneous Structure in Geodynamic Earth Models

Hans-Peter Bunge,* Mark A. Richards, Carolina Lithgow-Bertelloni, John R. Baumgardner, Stephen P. Grand, Barbara A. Romanowicz

Computer models of mantle convection constrained by the history of Cenozoic and Mesozoic plate motions explain some deep-mantle structural heterogeneity imaged by seismic tomography, especially those related to subduction. They also reveal a 150-million-year time scale for generating thermal heterogeneity in the mantle, comparable to the record of plate motion reconstructions, so that the problem of unknown initial conditions can be overcome. The pattern of lowermost mantle structure at the core-mantle boundary is controlled by subduction history, although seismic tomography reveals intense large-scale hot (low-velocity) upwelling features not explicitly predicted by the models.

Geodynamic Earth models were pioneered by Hager and O'Connell (*1*), who calculated mantle flow by imposing present-day plate motions as a surface boundary condition. With the advent of global seismic tomography (*2*), these models were extended to predict the geoid and dynamic topography (*3*). However, these Earth models are "static," because they solve for instantaneous mantle flow in response to boundary conditions, internal loads, or both.

Time-dependent Earth models are required to understand how the evolution of mantle flow affects Earth processes that occur on geologic time scales. For example, continental shelf and platform stratigraphy are controlled by vertical motions of the continental lithosphere in response to mantle convection (*4*). True polar wandering is caused by changes in the inertia tensor as a result of mantle convection (*5*), and the alternation between periods of rapid and slow magnetic field reversals is probably related to mantle-controlled changes at the core-mantle boundary (CMB).

The development of time-dependent Earth models has been delayed for several reasons: (i) Sufficient computer power to resolve the narrow thermal boundary layers in global mantle convection models has not been available; (ii) it is not obvious how the internal mantle density structure can be related to plate motion observations at the surface; and (iii) it is not known how time-dependent Earth models can be initialized at some starting point in the past, because the mantle density structure is known only for the present day (*6*).

Some of these difficulties have been overcome. (i) Advances in computer power allow three-dimensional (3D) spherical convection to be simulated at a resolution on the order of 50 to 100 km (*7, 8*). At the same time, large-scale mantle velocity heterogeneity structure has been mapped in greater detail (*9, 10*), and seismic tomography has imaged subducted slabs (*11–13*). (ii) The connection of internal mantle density structure to the history of subduction (*14, 15*) has allowed estimation of the internal buoyancy forces that drive plates (*16*). These developments allow convection models to be combined with plate motion reconstructions and such models to be tested with seismic data.

Figure 1B shows an Earth model obtained with the TERRA convection code (*17, 18*). More than 10 million finite elements provide an element resolution of about 50 km throughout the mantle, which allowed us to model convection at a Rayleigh number of 10^8 (*19*). The history of plate motion is imposed as a time-dependent velocity boundary condition (*20*) starting in the mid-Mesozoic at 119 to 100 million years ago (Ma). We chose this starting time because well-constrained reconstructions exist only as far back in time as the 119 to 100 Ma period.

In computing the Earth model (Table 1) we assumed that (i) the mantle is of uniform

H.-P. Bunge, Institut de Physique du Globe de Paris, Laboratoire de Sismologie, 4 place Jussieu, 75252 Paris Cedex 05, France.
M. A. Richards, Department of Geology and Geophysics, University of California, Berkeley, CA 94720, USA.
C. Lithgow-Bertelloni, Department of Geological Sciences, University of Michigan, Ann Arbor, MI 48109, USA.
J. R. Baumgardner, Theoretical Division, Los Alamos National Laboratory, Los Alamos, NM 87544, USA.
S. P. Grand, Department of Geological Sciences, University of Texas, Austin, TX 78713, USA.
B. A. Romanowicz, Berkeley Seismological Laboratory, and Department of Geology and Geophysics, University of California, Berkeley, CA 94720, USA.

*To whom correspondence should be addressed. E-mail: bunge@ipgp.jussieu.fr